

Tracing carbon dioxide fluxes from the Amazon River mouth into the Western Tropical North Atlantic using SMOS

A. M. Valerio^{1*}, M. Kampel¹, P. Yager², N. D. Ward³, H. O. Sawakuchi^{4,5}, A. C. Cunha⁶, A. V. Krusche⁵, J. E. Richey⁴

¹Remote Sensing Division, National Institute for Space Research, São José dos Campos, SP, Brazil

²Department of Marine Sciences, University of Georgia, Athens, GA, USA

³Marine Science Laboratory, Pacific Northwest National Laboratory, Sequim, Washington, USA

⁴School of Oceanography, University of Washington, Seattle, WA, USA

⁵Center of Nuclear Energy in Agriculture, University of São Paulo, Piracicaba, SP, Brazil

⁶Department of Environment and Development, Federal University of Amapá, Macapá, AP, Brazil

Corresponding author: Aline Valerio (alineval@dsr.inpe.br)

Key Points:

- Intra-annual variability was related mostly to rainfall and discharge at the Amazon River Mouth and liquid discharge, ocean currents, and trade winds in the plume.
- Inter-annual variability was a consequence of climatic events such as the severe drought throughout the Amazon basin in 2010 and record flood in 2012-2014.
- During the study period of 2010-2014, the Amazon River Plume acted as a source of CO₂ with an average annual flux of $5.64 \pm 7.2 \text{ Tg C y}^{-1}$.

Abstract

Constraining global carbon budgets requires a quantitative understanding of the evolving processes that occur along river to ocean gradients. However, high spatiotemporal resolution observations of these processes in large river systems are limited. Here we present in situ measurements of CO₂ concentrations made across the Amazon River mouth (ARM) and throughout the Amazon River Plume (ARP) during different discharge seasons from 2010-2012. Regressions models were used to estimate the partial pressure of CO₂ (pCO₂) and to determine temporal variability in CO₂ fluxes (F_{CO_2}) at the ARM as well as to derive the spatiotemporal distribution of pCO₂ using Soil Moisture and Ocean Salinity (SMOS) for each hydrologic period at the ARP. The estimation of pCO₂ and F_{CO_2} were extended for the years of 2013 and 2014. For the studied period, calculated F_{CO_2} for the ARP ranged from -0.203 to 0.502 $\mu\text{mol m}^{-2} \text{s}^{-1}$. The ARM was a source of CO₂ during all seasons with higher values of F_{CO_2} for the year of 2014 ($\mu=3.83 \pm 1.81 \mu\text{mol m}^{-2} \text{s}^{-1}$) and lower values for the year of 2010 ($\mu=2.91 \pm 1.51 \mu\text{mol m}^{-2} \text{s}^{-1}$). Intra-annual variability was related to rainfall and discharge at the mouth and ocean currents, and trade winds in the plume. Inter-annual variability was a consequence of climatic events such as the severe drought throughout the Amazon basin in 2010 and record flood in 2012-2014. For our study period the ARP acted as a source of CO₂ with an average annual flux of $5.64 \pm 7.2 \text{ Tg C yr}^{-1}$.

1 Introduction

Inland waters and coastal oceans are becoming increasingly recognized as an integrated water system through which geochemical constituents are constantly transformed providing unique biogeochemical influences in different sectors along the continuum [Hedges *et al.* 1997; Dagg *et al.*, 2004; Medeiros *et al.*, 2015; Ward *et al.*, 2015]. However, few studies have addressed the spatial and temporal dynamics of water and carbon fluxes from the mouth of major river systems out into marine receiving waters. While rivers usually act as a pump of CO₂ that transfers carbon dioxide from the water to the atmosphere [Cole *et al.*, 2007; Tranvik *et al.*, 2009; Raymond *et al.*, 2013] largely due to the breakdown of terrestrially-derived organic matter [Ward *et al.*, 2013] and floodplain inputs [Abril *et al.*, 2014], river-dominated coastal areas such as the Amazon River plume typically remove CO₂ from the atmosphere due to enhanced primary production driven by fluvial nutrients [Cooley *et al.*, 2007; Subramaniam *et al.*, 2008; Yeung *et al.*, 2012; Goes *et al.*, 2014].

Draining an area of ~6.5 million km², the Amazon basin represents 20% of all the freshwater discharge to the global ocean and ~25% of the global evasive CO₂ gas flux from inland waters [Richey *et al.*, 1990, 2002; Raymond *et al.*, 2013]. When flowing into the Western Tropical North Atlantic (WTNA), the dispersal of the Amazon River Plume (ARP) can extend offshore to an area of 10⁶ km² [Molleri *et al.*, 2010] and result in a carbon sequestration as high as ~27 Tg C yr⁻¹ from the atmosphere due to primary production in a mesohaline area (30-35) [Subramaniam *et al.*, 2008]. Lefèvre *et al.* [2010] estimated an annual CO₂ flux of 5 Tg C yr⁻¹ from the atmosphere into the ARP, whereas the Amazon River basin outgasses ~500 Tg C yr⁻¹ CO₂ from the river to the atmosphere [Richey *et al.*, 2002].

When the Amazon River reaches the ocean, it gathers with the North Brazil Current (NBC) and its waters are transported northwestward along the Brazilian Shelf in direction of the Guyana

Current. During the boreal summer to autumn period, a fraction of the ARP is retroflected and carried eastward by the North Equatorial Counter Current (NECC). During the boreal winter the water is trapped in the river mouth (recirculation current), due to the onshore trade winds against the coast [Lentz and Limeburner, 1995]. The seasonal behavior of the ARP has an ecological significance at the WTNA considering the response of the phytoplankton community to changing nutrients availability, and consequently affects the carbon dioxide flux [Cooley *et al.*, 2007; Subramaniam *et al.*, 2008].

Quantitative linkages between remotely sensed parameters and the partial pressure of CO₂ (pCO₂) has the potential to provide a synoptic view of these processes over a large spatial extent. Several studies have attempted to estimate pCO₂ from remote sensing and later compute the sea-air CO₂ flux. Sea Surface Temperature (SST) [Lohrenz and Cai, 2006; Zhu *et al.*, 2009; Bai *et al.*, 2015] and or chlorophyll-*a* concentration (chl-*a*) [Lohrenz and Cai, 2006; Zhu *et al.*, 2009; Hales *et al.*, 2012; Bai *et al.*, 2015] are usually the products retrieved by remote sensing that are used to relate by linear or multiple regression with in situ pCO₂. To improve the relationship, other parameters have been taken in account such as Sea Surface Salinity (SSS) [Bai *et al.*, 2015; Ibáñez *et al.*, 2015], wind [Zhu *et al.*, 2009] and colored dissolved organic matter (CDOM) [Lohrenz and Cai, 2006]. Besides the regression analysis, other methods such as principal component analysis [Lohrenz and Cai, 2006], neural networks [Landschützer *et al.*, 2014] and semi-analytical algorithms [Bai *et al.*, 2015] have also been applied in the literature.

The ability to estimate pCO₂ by satellite sensors allows a more holistic view of the variability and dynamics of sea-air CO₂ fluxes than in situ measurements alone and, as such, more accurate estimations of large-scale regional fluxes. Further, if the established relationship between pCO₂ and remotely sensed parameters is robust and well representative of a particular region beyond a particular sampling period, long term variability can be assessed both in present and in past times to assess the influence of environmental factors such as flood/drought cycles and decadal climate variations such as El Niño Southern Oscillation (ENSO) on CO₂ fluxes.

The aim of this study is to accurately quantify the flux of CO₂ to/from the atmosphere along the Amazon River continuum, from the actual river mouth (salinity = 0) out into the river plume and WTNA based on the correlation between remotely sensed parameter and in situ pCO₂ measurements. Here, we developed an algorithm to relate in situ pCO₂ measurements to remotely sensed parameters, SST and SSS, in order to evaluate the spatial distribution of pCO₂ along the continuum. Gas transfer velocities were then calculated across the study region based on a series of physical parameters (e.g. wind speed, SST, SSS) in order to evaluate the spatial distribution of CO₂ fluxes and ultimately quantify the overall flux of CO₂ to/from the atmosphere into the ARP water. Likewise, we quantified the evasive CO₂ flux from the river mouth (ARM) to the atmosphere and identified where in the plume CO₂ outgassing switches into CO₂ fixation from the atmosphere in an effort to view the integrated water system as a continuum.

2 Materials and Methods

2.1 Study Area

Two different sets of cruises were performed: 1) offshore of the Amazon River mouth and along its plume into the WTNA (defined in this study as 15°N-5°S; 60°W-45°W) and 2) in the lower Amazon River at the actual river mouth from 2010-2012. Six cruises were performed in the lower Amazon River across the river mouth, which is constrained by two main channels near the city of Macapá. At ARM, $p\text{CO}_2$ and discharge were measured at the Macapá North Channel (MNC) and Macapá South Channel (MSC) (00°05.400' S, 51° 03.200' W and 00°09.415' S, 50°37.353' W, respectively) (Figure 1a). The river cruises were carried out during the months of September (low water season) and December (early rising water season) of 2010, May (high water season) and September (low water season) of 2011 and April (late rising water season) and July (early falling water season) of 2012. The oceanographic cruises along the Amazon plume were performed during the months of May to June of 2010, September to October of 2011 and July of 2012. The set of months when data was collected represents the main hydrographic periods (Figure 1b). This study considers the river plume as the area covered by surface water with $\text{SSS} < 35$ for consistency with prior studies that established this threshold for the ARP [Coles *et al.*, 2013; Grodsky *et al.*, 2014; Ibáñez *et al.*, 2015; 2016]. In addition to the years of in situ sampling, we extended our study period for the years of 2013 and 2014.

The year of 2010 was characterized by a severe drought due to a strong El Niño [Marengo *et al.*, 2011] while the year of 2012-2014 was characterized by a record flood in the Amazon Basin that started with La Niña event in 2012 and continued with an anomalous SST in the tropical Atlantic south of the Equator and western tropical Pacific [Satyamurty *et al.*, 2013; Espinoza *et al.*, 2014; Marengo and Espinoza, 2016].

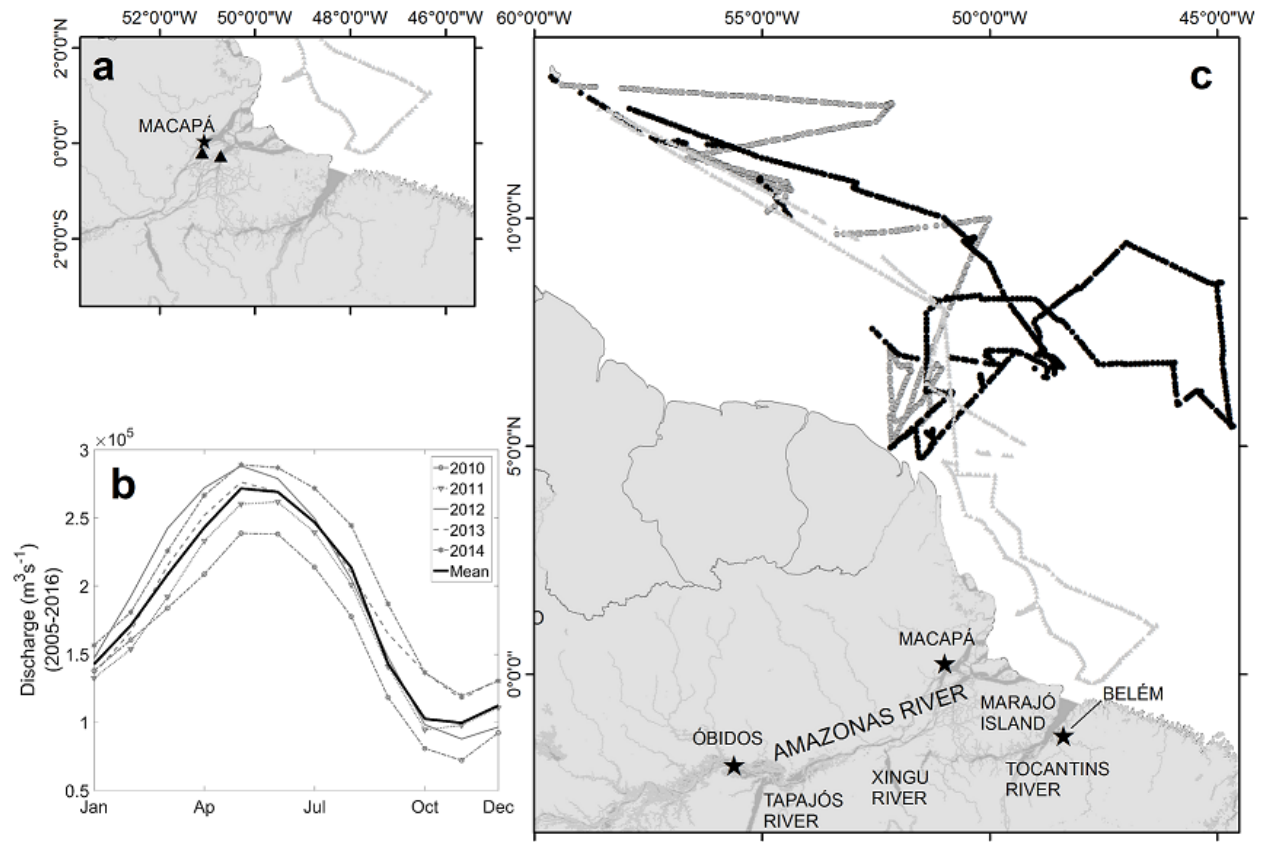


Figure 1. Study area. (a) Detail of the in situ sampling at the Amazon River mouth, at the north and south channels of Macapá. (b) Mean discharge (2005-2016) and discharge of the study years (2010-2014) of the Amazon River. Discharge data acquired from Óbidos station, from the National Agency of Waters of Brazil (ANA). (c) Overall study area showing the in situ sampling routes during the oceanographic cruises of 2010-2012.

2.2 Field measurements

SST and SSS were measured continuously during the three oceanographic cruises (R/V Knorr KN197 – June of 2010; R/V Melville MV1110 - September to October 2011; R/V Atlantis AT21-04 July of 2012) using the shipboard underway seawater system (Figure 1c). Surface $p\text{CO}_2$ during the oceanographic cruises was measured using an underway $p\text{CO}_2$ system with a non-dispersive infrared CO_2 gas analyzer (LI-COR 6252), and standardized using CO_2 -air reference gas mixtures from National Oceanic and Atmospheric Administration (NOAA) Climate Monitoring and Diagnostics Laboratory (CMDL). The in situ oceanographic data consists of 15,392 data points, taken every 10 minutes during the three cruises.

For the riverine $p\text{CO}_2$ measurements, a custom headspace equilibration chamber was used, based on *Frankignoulle et al.* [2001]. The equilibrator consists of a Plexiglas[®] vertical tube (height: 80 cm, diameter: 8 cm) filled with glass marbles to expand the exchange surface and to reduce air volume. Surface water was pumped from ~30 cm depth and flowed through the chamber, from the top to the bottom, at a rate of approximately 1.5 L min^{-1} . A smaller diaphragm pump provided a closed circuit of air (0.8 L min^{-1}) that circulates through the equilibrator (from bottom to top) and the flowing air is passed through a humidity trap (magnesium perchlorate), a desiccation tube containing a Drierite desiccant, and to an infrared CO_2 analyzer (LI-COR LI-820). The LI-820 was calibrated with the standard certificate of 420 (White Martins). Temperature was measured using an Orion 290Aplus probe submerged in a continuously overflowing graduated cylinder. River measurements at MNC and MSC were made at three cross-channel sampling sites dispersed equidistantly across each channel (i.e. left/right margin and center) [*Brito, 2013*], with values represented as the average of these measurements (36 samples total).

2.3 River discharge

River discharge was measured across the MNC and MSC during each of the six river cruises using a SonTek RiverSurveyor[®] M9 Portable nine-beam 3.0 MHz/1.0 MHz/0.5 MHz Acoustic Doppler Current Profiler (ADCP). Cross-channel ADCP transects were performed at approximately 1–2 h intervals for 10–13 h in order to assess river velocity over the span of an entire tidal cycle and calculate the total Amazon River discharge to the ocean. ADCP measurements of discharge were used to define the instantaneous discharge through each channel on the day of sampling. Likewise, an estimate of the proportional discharge from each channel was calculated based on these profiles (see more details in *Ward et al.* [2015]). This proportionality was applied to the river discharge data (2010-2014) calculated from the sum of discharges from various permanent stations, accessible from the National Agency of Waters of Brazil (ANA, <http://hidroweb.ana.gov.br>). The ANA stations used were Óbidos at the Amazon River, Itaituba at Tapajós River, and Altamira at the Xingu River. We excluded the contribution

from Tocantins River as it drains directly into the Atlantic Ocean near Belém, south of Marajó Island. Based on ADCP measurements it was determined that 40% of the total Amazon River flow (excluding the Tocantins River) flows through MNC and 60% flows through MSC (adapted from *Ward et al.* [2015]).

2.4 Remote sensing products

The Soil Moisture and Ocean Salinity (SMOS) mission measures microwave radiation emitted from the Earth's surface at 1.4 to 1.427 GHz, using an interferometric radiometer. SMOS was launched on November 2009 and in May 2010 started to provide data to the scientific community [Mecklenburg *et al.*, 2012; Reul *et al.*, 2012]. In this study, daily level 3 product with 0.5 degree of spatial resolution delivered by the Centre National d' Etudes Spatiales - Institut Français de Recherche pour l' Exploitation de la Mer (CNES- IFREMER) was used, which provides SSS, SST and Wind Speed (WS) data for the years of 2010-2014. SMOS products were acquired concomitantly to the oceanographic cruises (Table 1) also including ± 1 day around in situ sampling dates during the cruises of 2010-2012. This approach is justified to avoid missing data due to the 3 days revisit time of SMOS. Data from SMOS had preference in relation to Aquarius mission since it comprises the in situ sampling period of 2010-2012. Additionally, SMOS data has a better spatial resolution (0.5° rather than 1°), better revisit time (3 days rather than 7 days), and presented a better linear regression when compared to in situ surface salinity data (Aquarius: $N = 100$, $R^2 = 0.59$, RMSE 1.93; SMOS: $N = 253$, $R^2 = 0.66$, RMSE= 1.23) (Figure 2).

Table 1. Dates of the in situ sampling during riverine cruises at the Amazon River and oceanographic cruises at the Amazon plume.

| Oceanographic cruises | River cruises | |
|-----------------------|----------------------|----------------------|
| Amazon plume | North Macapá Channel | South Macapá Channel |
| 05-23 June 2010 | 16 Sep 2010 | 18 Sep 2010 |
| 02 Sep - 06 Oct 2011 | 01 Dec 2010 | 03 Dec 2010 |
| 13 - 29 Jul 2012 | 07 May 2011 | 09 May 2011 |
| | 13 Sep 2011 | 15 Sep 2011 |
| | 27 April 2012 | 29 April 2012 |
| | 23 July 2012 | 25 July 2012 |

SMOS products were further processed using the Sea-Viewing Wide Field-of View Sensor (SeaWiFS) Data Analysis System (SeaDAS) v. 7.3.1 software freely provided by NASA. All images were cropped for the WTNA area, and the math band function was used to calculate the $p\text{CO}_2$ and the sea-air CO_2 flux for the entire study area. The mosaic function was used for the three-month composite according to the Amazon River discharge season.

Although SMOS had a better performance than Aquarius in our study region, it still has drawback due to a higher microwave brightness temperature of the land, it contaminates the ocean signal leading to inaccurate SSS values [Talone *et al.*, 2009] and its use is restricted to beyond 100 km offshore. Furthermore, the choice to work with SMOS instead of a visible

sensor, was in consideration of the dataset that we have available. At the present, we do not have enough bio-optical properties data in that region to develop and validate a pCO₂ predictive algorithm using a visible sensor.

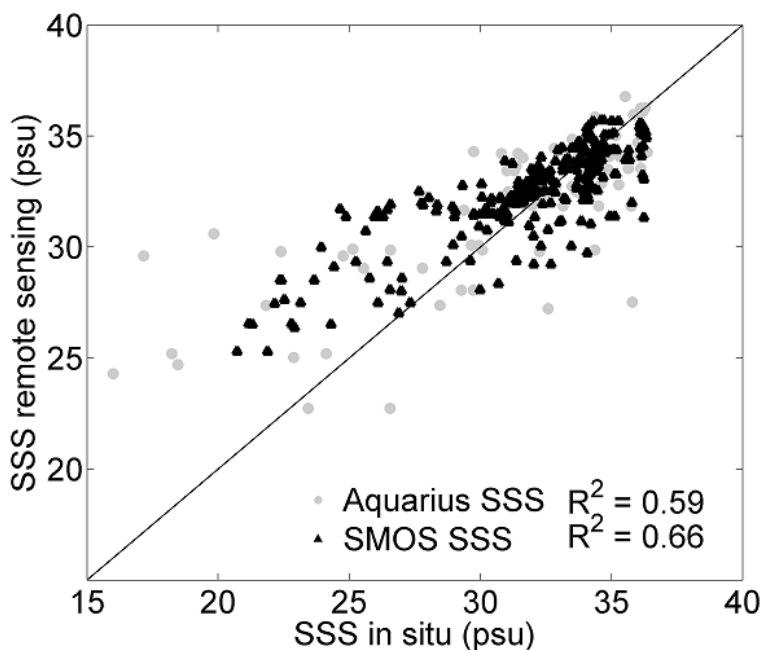


Figure 2. Linear regression between in situ sea surface salinity and SSS estimated by remote sensing, using Aquarius and SMOS data (N = 100, $R^2 = 0.59$, RMSE 1.93; N= 253, $R^2 = 0.66$, RMSE= 1.23, respectively).

2.5 pCO₂ predictive algorithm

A predictive algorithm for the WTNA was developed exploring the relation between in situ SSS, SST and pCO₂ data using a multiple polynomial regression model (MPR). SSS and SST have been described to have a relationship with the variability of pCO₂ at the ARP, although the relationship between SSS and pCO₂ is much more evident [Ternon *et al.*, 2000]. Despite in the literature there are different approaches to estimate and map the pCO₂, they are all relatively consistent with previous estimations for the same region and season [Rödenbeck *et al.*, 2015]. Later, SSS, SST and pCO₂ measurements along the three oceanographic cruises were averaged for every pixel of the SMOS daily products (N= 318), and from now on these variables will be here denominated as SSS_a, SST_a and pCO_{2a}. The variability of these in situ data within the SMOS pixel was calculated as the coefficient of variation:

$$cv = \frac{\sigma}{\mu} \quad (\text{Eq. 1})$$

where σ is the standard deviation and μ is the average of all in situ data within the SMOS pixel.

Outliers were removed after a Cook's distance analysis, limiting to 253 samples, where 70% of the samples were partitioned to generate the model using the MPR and 30% were used for validation (N_{model}=177; N_{validation} = 76). The resultant formula was applied to SMOS daily data

of the same dates of in situ sampling to generate pCO₂ remote sensing products and to validate the model. Later, the predictive algorithm was applied to three months' composites of SMOS data for the years of 2010-2012. Unfortunately, to develop the model, the samples from 2012 obtained at less than 100 km from the shoreline were excluded because they were outside the limits of SMOS products.

To predict the pCO₂ of the ARM, a linear regression was calculated between in situ pCO₂ measurements and river discharge. This linear model was applied to the sum of daily river discharge during 2010-2012, acquired from ANA. The resulting pCO₂ data was averaged for each three-month discharge season.

2.6 Sea-air CO₂ flux

The sea-air CO₂ flux, $F_{CO_2}^{sea}$ ($\mu\text{mol m}^{-2} \text{s}^{-1}$) in the WTNA and at the ARM, $F_{CO_2}^{river}$ ($\mu\text{mol m}^{-2} \text{s}^{-1}$), were calculated according to Wanninkhof [1992]:

$$F_{CO_2} = k_{CO_2} K_0 (pCO_2^{water} - pCO_2^{air}) \quad (\text{Eq. 2})$$

where pCO₂ is the partial pressure of CO₂ (μatm), k_{CO_2} (cm hr^{-1}) is the gas transfer coefficient and K_0 is the solubility of CO₂. Negative values of F_{CO_2} indicate that the water acts as a carbon sink while positive values indicate that water acts as a source of carbon to the atmosphere. pCO_2^{air} was obtained from Barbados (13.17°N-59.43°W), the closest station of the NOAA Earth System Research Laboratory (ESRL) Global Monitoring Division.

The gas transfer coefficient, k_{CO_2} (cm hr^{-1}) was calculated as a function of wind speed, but this relationship is geographically restricted for the study area [Borges *et al.*, 2004]. For that reason, we calculated k_{CO_2} specifically for the river area and for the ARP.

For the ARP, k_{CO_2} was calculated as a quadratic function of wind speed (m s^{-1}) updated by Wanninkhof [2014] which has a 20% uncertainty:

$$k_{CO_2}^{sea} = 0.251 U_{10}^2 \left(\sqrt{\frac{660}{Sc}} \right) \quad (\text{Eq. 3})$$

For the Amazon River mouth, k_{CO_2} was calculated as a linear function of wind speed based on extensive measurements in the Amazon and Mekong river (latter river not shown in Figure1) systems [Alin *et al.*, 2011]:

$$k_{CO_2}^{river} = 4.46 + 7.11 U_{10} \quad (\text{Eq. 4})$$

where U_{10} is the wind speed (m s^{-1}) at 10 m above the water surface and Sc is the Schmidt dimensionless number determined as follows [Wanninkhof, 2014]:

$$Sc = A + B(T) + C(T^2) + D(T^3) + E(T^4) \quad (\text{Eq. 5})$$

Where T is the water temperature (°C). The values of A, B, C, D and E for the sea are presented in Table 2. For $F_{CO_2}^{sea}$, the T and U_{10} were obtained from the SMOS data. For $F_{CO_2}^{river}$, U_{10} were obtained from a meteorological station at Macapá (00.05°S-51.11°W, station 82098) available at the National Institute of Meteorology of Brazil (INMET, <http://www.inmet.gov.br>). The temperature of the river was measured in situ at the same day of pCO₂ and discharge measurements.

Table 2. Coefficients of Schmidt Number for ocean for temperatures ranging from -2 to 40° [Wanninkhof, 2014]

| | Ocean |
|---|-----------|
| A | 2116,8 |
| B | -136,25 |
| C | 4,7353 |
| D | -0,092307 |
| E | 0,000756 |

To convert partial pressures into molar units, the solubility of CO₂, K_0 (mol L⁻¹ atm⁻¹) was calculated according to Weiss [1974]:

$$K_0 = e^{\left[-58.0931+90.5069\left(\frac{100}{K}\right)+22.294 * \ln\left(\frac{K}{100}\right)+0.027766*S-0.025888*S\left(\frac{K}{100}\right)+0.0050578*S\left(\frac{K}{100}\right)^2\right]} \quad (\text{Eq. 6})$$

where K is the water temperature in Kelvin. For the calculation of K_0 for the river data, the salinity effect was dismissed. All formulae to calculate F_{CO_2} , k , Sc and K_0 were applied to the SMOS seasonal discharge composites.

3 Results and discussion

3.1 Synthetic pCO₂ for the WTNA

In situ measurements of SST and SSS had a significant correlation with pCO₂ along the oceanographic cruise boundaries (Figure 3a) (N= 159392, $R^2 = 0.76$, $p < 0.005$, RMSE = 51.95 µatm). Most of the in situ pCO₂ measurements along the WTNA ranged between 120-500 µatm; these values are similar to measurements shown by Cooley *et al.* [2007]. When pCO₂ reaches higher values (> 500 µatm), the relationship between SST, SSS and pCO₂ tends to be weaker, suggesting that another variable has an important influence at this interval. The relationship become stronger again when pCO₂ reaches values higher than 750 µatm. The weakness of the relationship is likely due to a strong influence of the river. When all the three cruises in situ data are gathered (Figure 3b), it is possible to see two very distinct water masses: river and ocean. The river water has higher pCO₂ and it is concentrated in the higher scatter interval (Figure 3a).

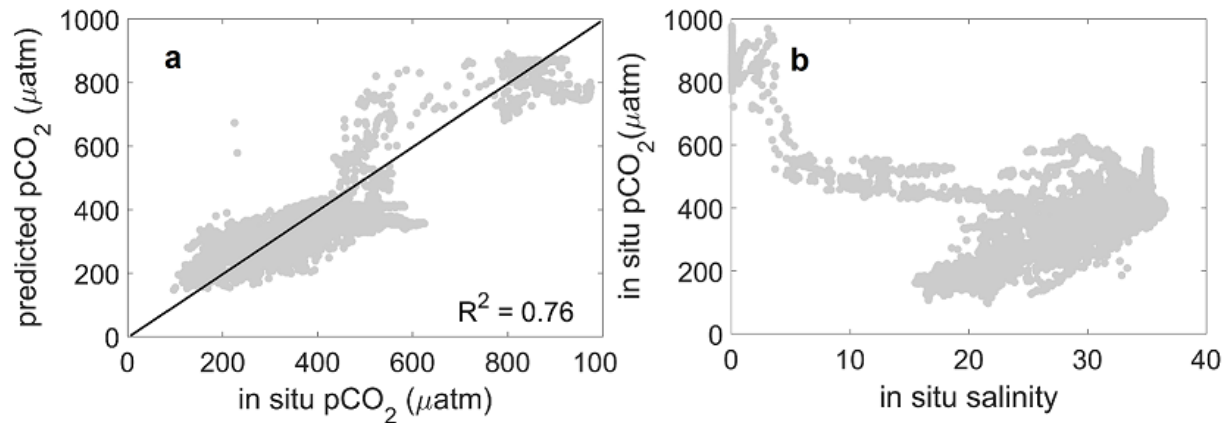


Figure 3. (a) Multiple polynomial regression between in situ SSS, SST and pCO₂ (N = 15392, R² = 0.76, RMSE = 51.95 μatm, p < 0.005). (b) Correlation between in situ salinity and in situ pCO₂ (N=15392).

This behavior illustrates the difficulty in predicting pCO₂ through a large spatial-time scale and the SSS and SST tends to overestimate pCO₂ at this scattering interval. Although all three cruises were passing by within the Amazon plume, they had different routes as can be seen in Figure 1c. The cruise of 2012 was much closer to the coast and the pCO₂ values are much higher when compared to the others two cruises (Table 3).

Table 3. Basic statistics of in situ pCO₂ sampled during the three oceanographic cruises (2010-2012).

| Sampling years of pCO ₂ (μatm) | Min | Max | Mean |
|---|--------|--------|-----------------|
| 2010 | 107 | 477 | 320.44 ± 76.59 |
| 2011 | 126.34 | 477.52 | 348.99 ± 40.59 |
| 2012 | 152.49 | 976.04 | 396.45 ± 129.33 |

To match the SMOS pixel spatial resolution of 0.5°, in situ data were averaged and after a Cook's analysis, some outliers were discarded. Basic statistics calculated before and after the averaging are shown in Table 4. Even though it is necessary to average a great number of in situ data points, the coefficient of variation shows consistent values of SSS, SST and pCO₂ within each pixel.

Table 4. Statistics and coefficient of variation of the variables used to develop the model for the Amazon River Plume, before and after averaging to match the SMOS spatial resolution of 0.5°.

| Variable name | Variable description | Min | Max | Mean | C.V. min (%) | C.V. max (%) | C.V. mean (%) |
|---------------|----------------------|-----|-----|------|--------------|--------------|---------------|
|---------------|----------------------|-----|-----|------|--------------|--------------|---------------|

| | | | | | | | |
|--------------------------|--|-------|--------|---------------------|-------|------|-----|
| SSS in situ | In situ salinity measured at surface during three oceanographic cruises | 0.043 | 36.52 | 30.23 ± 6.92 | -- | -- | -- |
| | In situ temperature measured at surface during three oceanographic cruises | 26.89 | 30.82 | 29.05 ± 0.66 | -- | -- | -- |
| SST in situ (°C) | In situ pCO ₂ measured at surface during three oceanographic cruises | 96.72 | 976.04 | 370.62 ± 106.59 | -- | -- | -- |
| | In situ salinity measured at surface during three oceanographic cruises, averaged to match the SMOS spatial resolution of 0.5° | 20.73 | 36.34 | 31.81 ± 3.45 | 0.002 | 20.2 | 1.6 |
| SST _a (°C) | In situ temperature measured at surface during three oceanographic cruises, averaged to match the SMOS spatial resolution of 0.5° | 27.1 | 30.43 | 29.20 ± 0.65 | 0.007 | 3.5 | 0.3 |
| | In situ pCO ₂ measured at surface during three oceanographic cruises, averaged to match the SMOS spatial resolution of 0.5° | 150.1 | 432.97 | 349.1 ± 49.40 | 0.03 | 21.3 | 2.8 |
| pCO _{2a} (µatm) | | | | | | | |

The SSS_a and SST_a values used to generate the model were linearly correlated to SMOS, SSS, and SST (Figure 4a and Figure 4b, respectively) and it is possible to observe that SMOS products typically presents higher values of salinity when SSS is under 30 as well as the satellite sensor has a bias of underestimating the in situ SST. *Reul et al.* [2012] has also observed a SSS bias where SMOS data are too salty in coastal waters where the salinity measured in situ is below 33.

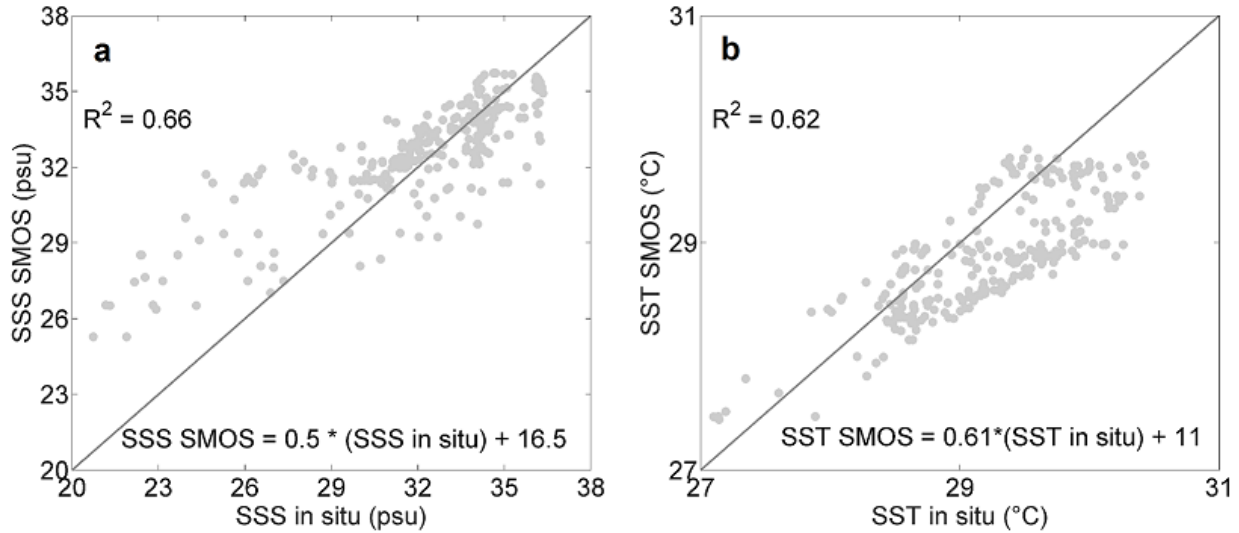


Figure 4. Linear relationship between: a) in situ SSS_a and SMOS SSS ($N = 176$, $R^2 = 0.66$, $RMSE = 1.23$, $p < 0.005$); b) SST_a and SMOS SST ($N = 176$, $R^2 = 0.62$, $RMSE = 0.31$ °C, $p < 0.005$).

This complication added to the land contamination is crucial for the use of SMOS products to study the ARP especially when it is very close to the ARM. Applying the MPR to SMOS-derived SSS and SST it was possible to generate an empirical function to estimate pCO_2 as follows:

$$pCO_2 = 0.05 (SSS)^2 + 34.81(SST)^2 + 19.71(SSS * SST) + 48792.07 - 560.47(SSS) - 2694.56(SST) \quad (\text{Eq. 7})$$

The empirical model was satisfactorily validated (Figure 5a, $N = 76$, $R^2 = 0.74$, $RMSE = 30$ μatm , $p < 0.005$), although the model presented an issue with an underestimation of values below 300 μatm . pCO_2 values < 300 μatm were correlated with salinities < 30 , in the range of 20 to 35 (Figure 5b), and, as shown previously, SMOS had problems estimating SSS under this threshold. Nevertheless, the model accurately represented the pCO_2 distribution throughout ARP (Figure 5c).

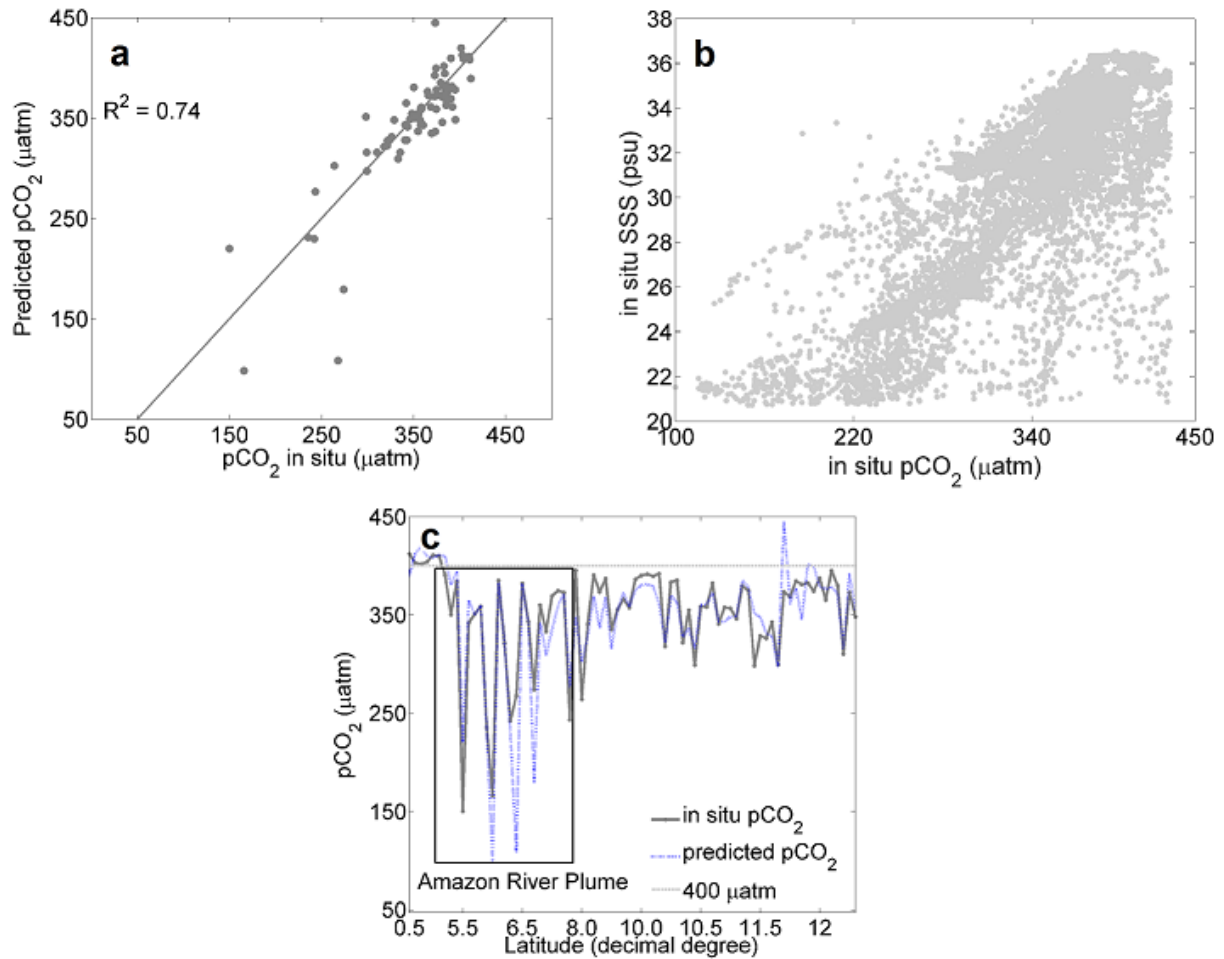


Figure 5. (a) Validation of the Multiple polynomial regression function of SMOS-derived SSS and SST to estimate $p\text{CO}_2$ at the Amazon River plume ($N = 76$, $R^2 = 0.74$, $\text{RMSE} = 30 \mu\text{atm}$, $p < 0.005$); (b) Correlation between in situ SSS and $p\text{CO}_2$ within the interval of 150–450 μatm ; (c) Latitudinal distribution of in situ $p\text{CO}_2$ and estimated- $p\text{CO}_2$ for the WTNA area with SMOS products.

For validation, the $p\text{CO}_2$ function was applied to a composition of three months of SMOS products, according to the seasonal discharge of the Amazon River (Figure 6). The ARP is very distinct from the surrounding water of the WTNA, with comparatively lower values of estimated $p\text{CO}_2$, ranging between 65–850 μatm ($\mu = 406 \pm 24 \mu\text{atm}$) during the five years (Table 5).

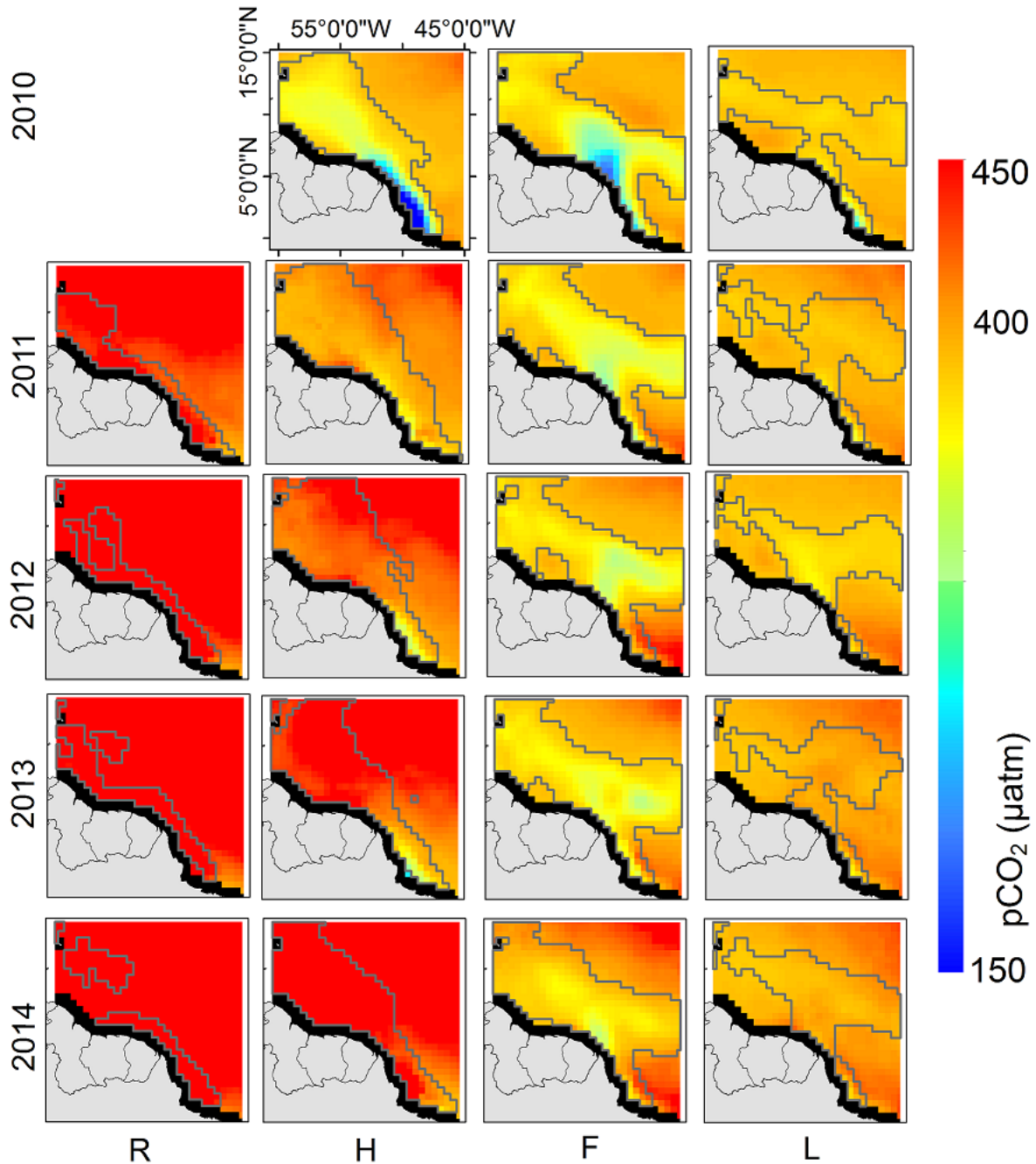


Figure 6. Estimated- $p\text{CO}_2$ for the WTNA area with SMOS products for the discharge season: Rising (January, February, March), High (April, May, June), Falling (July, August, September) and Low water (October, November and December) for the years of 2010-2014. The gray line refers to the ARP and the black area refers to no data.

Our results agree with other $p\text{CO}_2$ values derived from remote sensing studies in coastal areas dominated by rivers, where the mixing between river and ocean waters decreases $p\text{CO}_2$ values observed at the plume, probably due to biological uptake [Lohrenz and Cai, 2006; Bai et al., 2015]. During the rising water season the WTNA had relatively higher $p\text{CO}_2$ values perhaps due

to the imprisonment of ARP close to the river mouth, which decreases the input of nutrients into the ocean. Likewise, pCO₂ values in the river are generally higher during rising and high water periods [Richey *et al.*, 2002], meaning that large amounts of CO₂-rich waters are exported from the river to the ocean during rising water season. During the high water season the ARP is driven northwestwards by the NBC, and during the falling water season a retroflexion of the ARP has been observed driving nutrient-rich waters eastwards [Lentz and Limeburner, 1995] and leading to lower values of pCO₂ due to biological uptake. The overall seasonal pCO₂ values obtained in our study in the ARP are similar to previously reported by Cooley *et al.* [2007] and Ibáñez *et al.* [2016], although we also observed higher values (> 500 µatm) during the rising water season of 2011 and 2012 and during the rising and high water of 2013 and 2014 (Table 5). The high water season of 2010 was not represented in our spatial analyses because SMOS mission only began providing data in May of 2010.

Table 5. Statistics for the estimated pCO₂ (µatm) for the Amazon River Plume.

| Year | Seasonal Discharge | Min | Max | Mean |
|------|--------------------|--------|--------|----------------|
| 2010 | High | 65 | 380.71 | 338.17 ± 55.22 |
| | Falling | 192.44 | 384.41 | 341.97 ± 38.79 |
| | Low | 247.5 | 380.93 | 369.05 ± 12.91 |
| 2011 | Rising | 382.2 | 576.31 | 451.88 ± 27.69 |
| | High | 324.59 | 428.8 | 389.01 ± 14.20 |
| | Falling | 285.43 | 411.73 | 353.17 ± 19.75 |
| | Low | 338.29 | 396.53 | 377.24 ± 6.28 |
| 2012 | Rising | 408.73 | 599.63 | 489.76 ± 30.29 |
| | High | 313.33 | 479.98 | 418.96 ± 27.72 |
| | Falling | 302.79 | 438.8 | 358.80 ± 22.61 |
| | Low | 348.43 | 404.8 | 368.28 ± 6.80 |
| 2013 | Rising | 426.75 | 553.50 | 474.27 ± 20.26 |
| | High | 290.29 | 509.66 | 436.84 ± 36.62 |
| | Falling | 305.26 | 422.61 | 358.18 ± 15.79 |
| | Low | 350.21 | 407.83 | 386.90 ± 7.71 |
| 2014 | Rising | 440.77 | 841.24 | 561.87 ± 49.26 |
| | High | 358.11 | 545.04 | 479.89 ± 35.49 |
| | Falling | 307.91 | 436.51 | 373.08 ± 17.98 |
| | Low | 367.79 | 421.20 | 385.06 ± 8.80 |

3.2 Synthetic pCO₂ for the Amazon River mouth

The relationship between $p\text{CO}_2$ and river discharge in Amazonian waters has been described by *Richey et al.* [2002] as well as the wide range of $p\text{CO}_2$ values for many tributaries and mainstem river of the Amazon Basin. The wide range of $p\text{CO}_2$ throughout the Amazon basin is related to the physiochemical characteristics of the watershed, according to the course of each river in their respective environment as well as the mixing waters of their tributaries [*Rasera et al.*, 2013]. For this reason, we considered important to study separately the MNC and MSC contributions to the flux of CO_2 . Significant linear relationships between $p\text{CO}_2$ and in situ measured discharge at the MNC ($N = 6$, $R^2 = 0.96$, $\text{RMSE} = 286.2 \mu\text{atm}$, $p < 0.005$) and MSC ($N = 6$, $R^2 = 0.89$, $\text{RMSE} = 408.6 \mu\text{atm}$, $p < 0.005$) were obtained (Figure 7), and the following empirical functions were calculated as follows:

$$p\text{CO}_{2\text{north}} = 0.03764(Q) - 94.54 \text{ (Eq. 8)}$$

$$p\text{CO}_{2\text{south}} = 0.02452(Q) - 273.2 \text{ (Eq. 9)}$$

where Q is the discharge ($\text{m}^3 \text{s}^{-1}$).

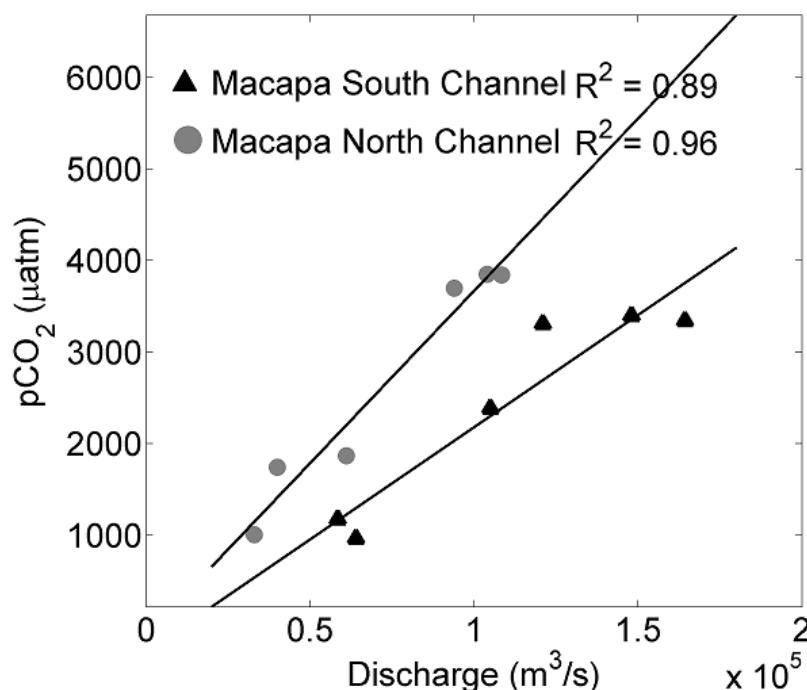


Figure 7. Linear relationship between the $p\text{CO}_2$ and discharge measured in situ at the South and North Channels of the Amazon River mouth ($p\text{CO}_2$ North: $N = 6$, $R^2 = 0.95$, $\text{RMSE} = 286.2 \mu\text{atm}$, $p < 0.005$; $p\text{CO}_2$ South: $N = 6$, $R^2 = 0.89$, $\text{RMSE} = 408.6 \mu\text{atm}$, $p < 0.005$).

After partitioning daily ANA discharge data into MNC and MSC (40% MNC, 60% MSC), these $p\text{CO}_2$ functions were applied for a 2010-2014 time-series (Figure 8) with values ranging between 1134 and 5084 μatm for the MNC ($\mu = 3077 \pm 1152 \mu\text{atm}$) and 927 to 4787 μatm for the MSC ($\mu = 2826 \pm 1125 \mu\text{atm}$). The ARM was supersaturated in $p\text{CO}_2$ during all periods and the highest values were observed during April (late rising to high water period) while the lowest values were

estimated during October–November (low water period). Our $p\text{CO}_2$ estimates for the ARM are lower than the reported for the Central Amazon Basin [Richey *et al.*, 2002; Lauerwald *et al.*, 2015]. Although there are continuous inputs of CO_2 and reactive organic matter along the downstream gradient, degassing appears to be faster than these inputs. A similar downstream decrease in $p\text{CO}_2$ along the Central Amazon River was observed by Abril *et al.* (2014) with floodplains and upstream rivers and their channels displaying higher saturation values compared to downstream open lakes and Amazon River channels.

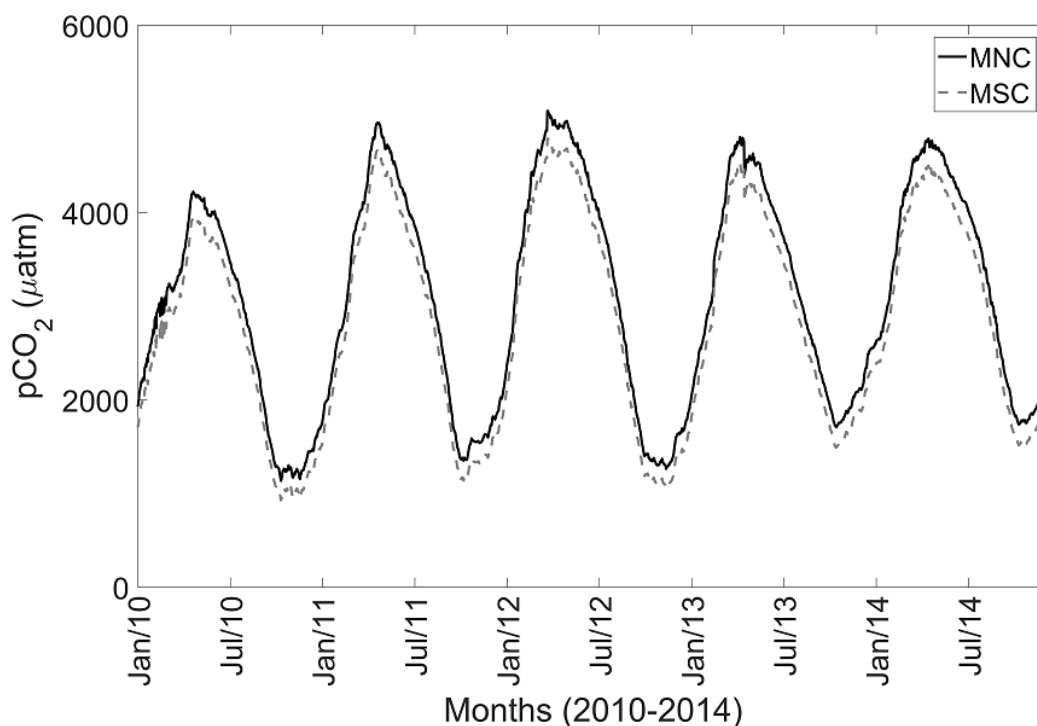


Figure 8. Estimated $p\text{CO}_2$ for the Macapá North Channel (solid line) and Macapá South Channel (dashed line) for the period of 2010–2014.

The year of 2010 presented lower values of $p\text{CO}_2$ compared to 2011–2014. This pattern is connected to the extreme drought of 2010 in the Amazon region, in which the main tributaries of the Amazon River had the lowest water level and isolated some regions where streams were completely dried up [Marengo *et al.*, 2011]. Therefore, the input of gaseous and organic carbon to the mainstem was also diminished. More details on the evolution of $p\text{CO}_2$ and directly measured CO_2 outgassing fluxes along the lower Amazon River, from Óbidos to the river mouth are provided by Sawakuchi *et al.* [in review].

3.3 Water-air CO_2 flux for the Amazon Continuum

Calculated monthly sea-air CO_2 fluxes for the ARP ranged from $-0.203 \mu\text{mol m}^{-2} \text{s}^{-1}$, during the high water period of 2010 to $0.502 \mu\text{mol m}^{-2} \text{s}^{-1}$ during the rising water period of 2014 (Table 6).

Table 6. Statistics for the Sea-air CO₂ flux ($\mu\text{mol m}^2 \text{s}^{-1}$) for the Amazon River Plume.

| Year | Seasonal Discharge | Min | Max | Mean |
|------|--------------------|--------|--------|--------------------|
| 2010 | High | -0.203 | -0.005 | -0.041 ± 0.032 |
| | Falling | -0.117 | -0.002 | -0.026 ± 0.021 |
| | Low | -0.115 | -0.005 | -0.016 ± 0.010 |
| 2011 | Rising | -0.004 | 0.155 | 0.08 ± 0.031 |
| | High | -0.047 | 0.047 | -0.003 ± 0.015 |
| | Falling | -0.088 | 0.025 | -0.022 ± 0.013 |
| | Low | -0.055 | 0.011 | -0.010 ± 0.006 |
| 2012 | Rising | 0.020 | 0.353 | 0.139 ± 0.049 |
| | High | -0.069 | 0.138 | 0.046 ± 0.038 |
| | Falling | -0.046 | 0.053 | -0.016 ± 0.013 |
| | Low | -0.031 | 0.010 | -0.016 ± 0.005 |
| 2013 | Rising | 0.047 | 0.206 | 0.123 ± 0.030 |
| | High | -0.074 | 0.204 | 0.078 ± 0.055 |
| | Falling | -0.062 | 0.029 | -0.019 ± 0.010 |
| | Low | -0.042 | 0.022 | -0.001 ± 0.010 |
| 2014 | Rising | 0.055 | 0.502 | 0.270 ± 0.072 |
| | High | -0.026 | 0.258 | 0.143 ± 0.063 |
| | Falling | -0.054 | 0.058 | -0.011 ± 0.016 |
| | Low | -0.024 | 0.035 | -0.003 ± 0.010 |

In general, during the rising water season the WTNA was a source of CO₂ to the atmosphere, likely due to the imprisonment of the CO₂-rich Amazon River water that was trapped against the coast (Figure 9). Even within the Amazon plume, patches has acted as a source of CO₂. The behavior of the $F_{\text{CO}_2}^{\text{sea}}$ was very similar from the pCO₂ and it suggests that the pCO₂ is the main driver of the CO₂ flux in this region rather than variable wind speed. It is interesting to note that during 2010 the ARP had the lowest values of $F_{\text{CO}_2}^{\text{sea}}$, acting as a bigger sink of atmospheric CO₂ comparing to the others study years.

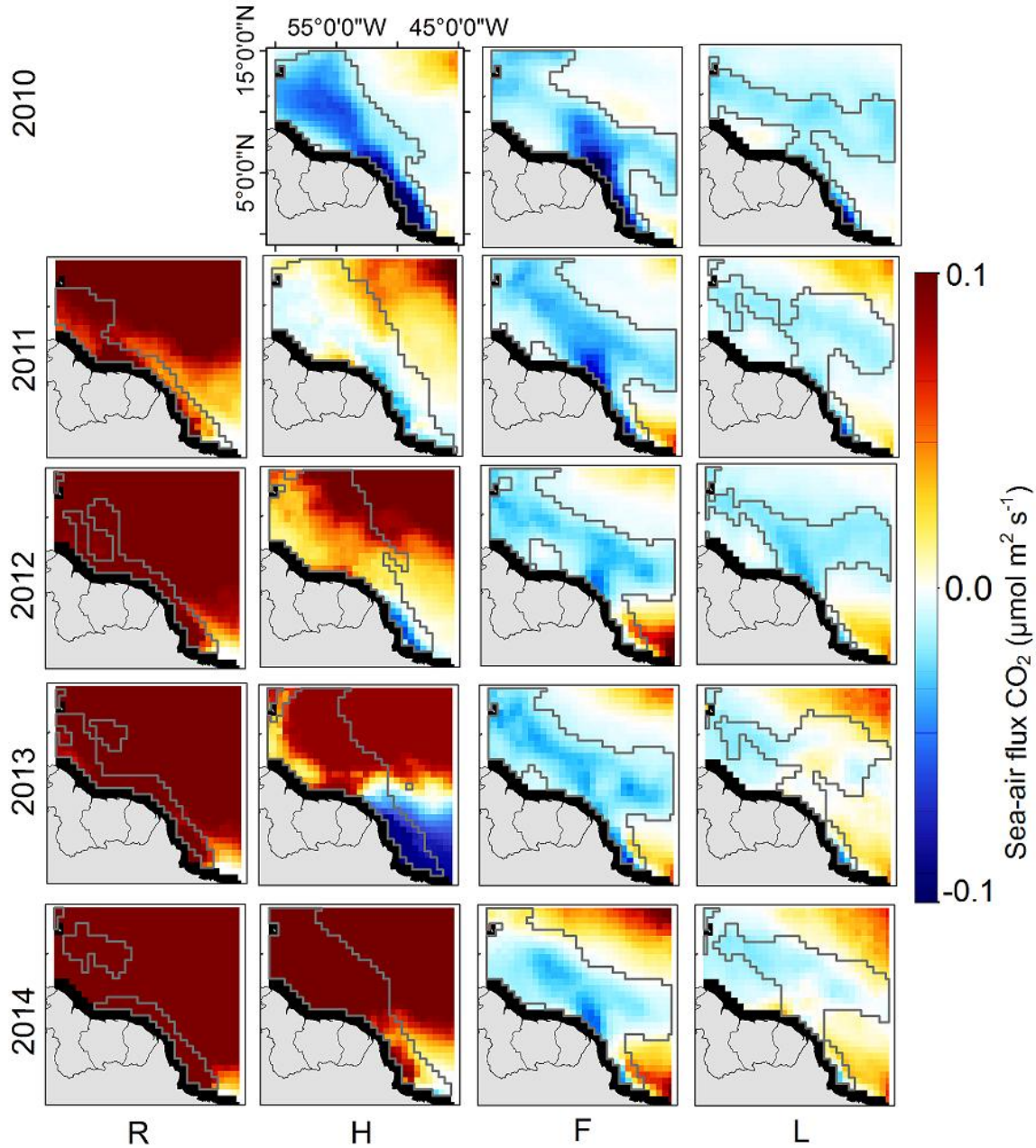


Figure 9. Sea-air CO_2 flux ($\mu\text{mol m}^{-2} \text{s}^{-1}$) estimated for the WTNA area with SMOS products for the discharge season: Rising (January, February, March), High (April, May, June), Falling (July, August, September) and Low water (October, November and December) for the years of 2010-2014. The gray line refers to the ARP and the black area refers to no data.

On the other hand, 2014 had the highest values of $F_{\text{CO}_2}^{\text{sea}}$ (Figure 10). These two contrasting years were marked by a severe drought and a significant flood, respectively, illustrating the dependence of plume dynamics on large-scale hydrologic patterns. This is highly relevant to future projections of carbon cycling in the region and globally considering climate change is expected to enhance flood/drought cycles [Nohara *et al.*, 2006].

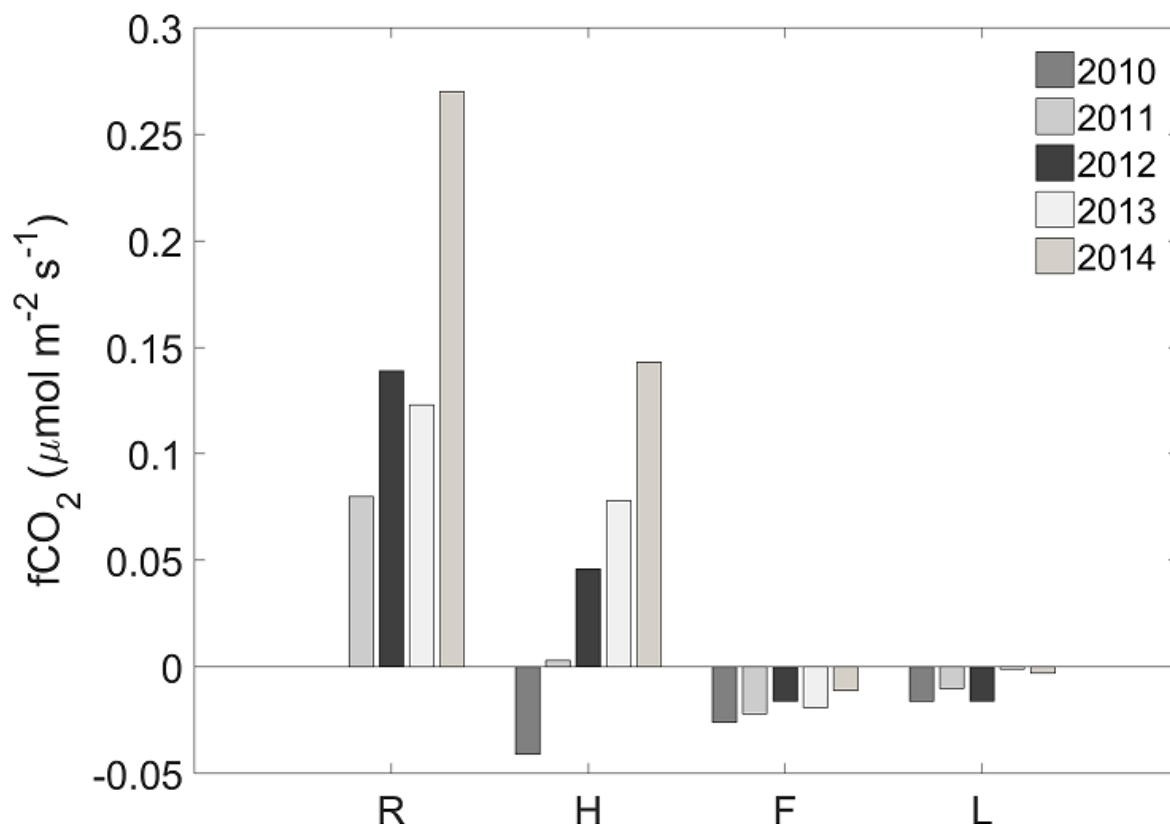


Figure 10. Average of all sea-air CO₂ flux for the Amazon River Plume area with SMOS resolution of 0.5° for the discharge season: Rising (January, February, March), High (April, May, June), Falling (July, August, September) and Low water (October, November and December) for the years of 2010-2014.

Our results are in agreement with values presented by *Ibáñez et al.* [2015] (-0.127 to $0.034 \mu\text{mol m}^{-2} \text{s}^{-1}$) also indicating that most of the CO₂ outgassing occurs in lower latitudes. Likewise, both results agree that the highest levels of CO₂ outgassing in the tropical Atlantic occur during the rising water period, whereas the highest levels of CO₂ uptake occur during low water. In our study, the Amazon River was a source of CO₂ during all periods with higher values of $F_{\text{CO}_2}^{\text{river}}$ in 2014 ($\mu=3.83 \pm 1.81 \mu\text{mol m}^{-2} \text{s}^{-1}$, average for both channels) and lower values in 2010 ($\mu=2.91 \pm 1.51 \mu\text{mol m}^{-2} \text{s}^{-1}$, average for both channels). For all years, the high water season was marked by high $F_{\text{CO}_2}^{\text{river}}$ ($\mu=4.42 \pm 0.57 \mu\text{mol m}^{-2} \text{s}^{-1}$, average for all high water seasons for both channels) while the low water season presented the lowest $F_{\text{CO}_2}^{\text{river}}$ values ($\mu=2.24 \pm 0.58 \mu\text{mol m}^{-2} \text{s}^{-1}$, average for all low water seasons for both channels). MSC contributes more to the total flux of water to the plume relative to MNC (60% and 40%, respectively). Thus, considering the major contribution of the MSC to the river discharge and its average pCO₂ was only 9% lower compared to MNC, the MSC contributes to a larger proportion of the overall flux of CO₂ to the ARP. Comparing the observed concentrations and fluxes at the Amazon mouth with values from other Amazonian rivers (e.g., Negro, Solimões, Araguaia – not shown in Figure 1) [Rasera et al, 2013] it is possible to show that our results are lower most likely due to continuous degassing

along the continuum that occurs faster than replenishment by CO_2 and reactive organic matter inputs. Furthermore, the lower fluxes compared to others Amazonian rivers could be also related to the dilution by lowland tributaries such as the Tapajós and Xingu rivers, which have high levels of primary production, and are at some times close to atmospheric CO_2 saturation [Ward *et al.*, 2015; 2016].

It is important to note the synergy between the ARP and the Amazon River. For example, when the river has lower $F_{\text{CO}_2}^{\text{river}}$, the plume sinks more CO_2 . When the river has higher values of $F_{\text{CO}_2}^{\text{river}}$, the plume sinks less CO_2 , and depending on how much CO_2 is emitted from the river, the ARP acts also as a source of CO_2 (Figure 10 and Figure 11). This phenomenon is directly linked to the hydrology of the Amazon basin.

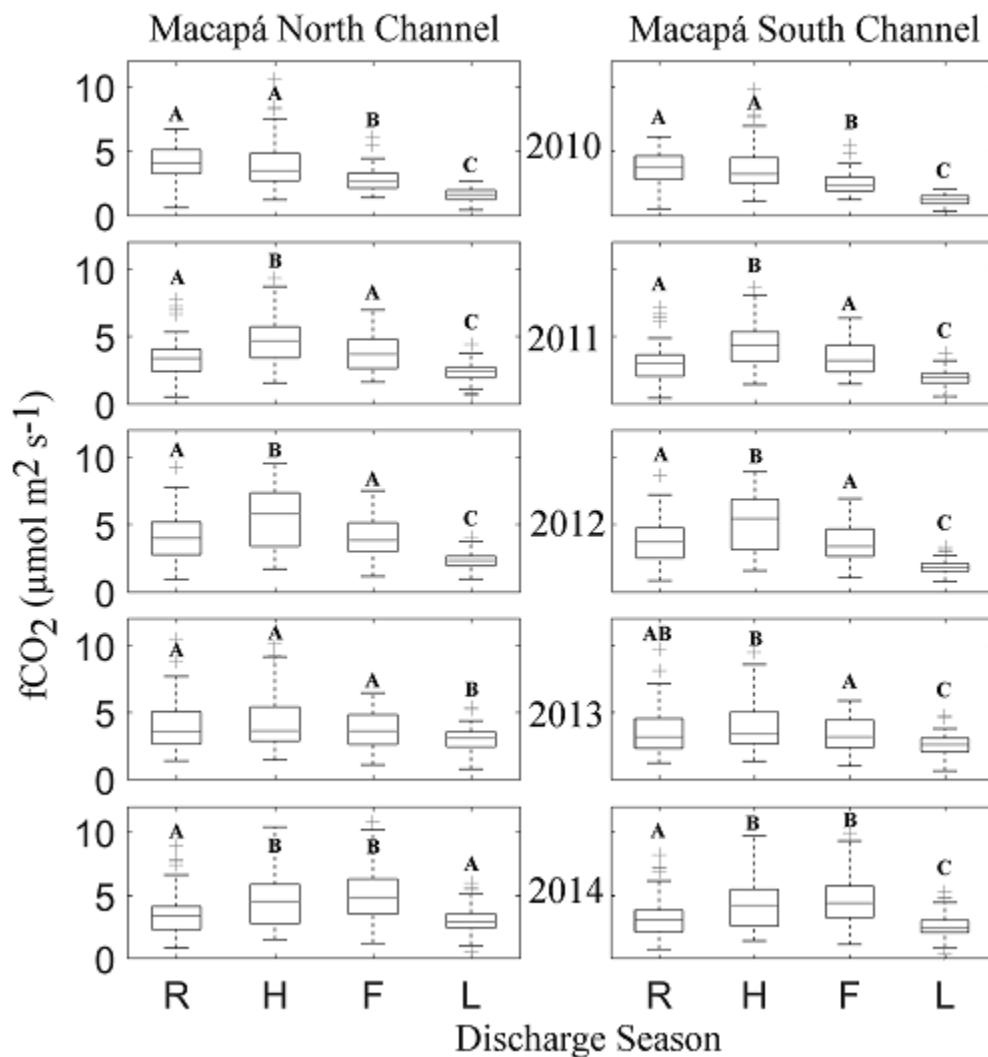


Figure 11. Box-plot of the river-air CO_2 flux during the discharge season for the years of 2010-2014 for the North and South Macapá Channels. The outliers are plotted using the '+' symbol. Letters show the results for multiple pair-wise comparisons of group means using Tukey's range

test. Variables which do not share a letter have significantly different mean importance ($p < 0.05$).

3.4 Annual flux of CO₂ in the Amazon River Plume

The average annual flux of CO₂ for the entire plume during our study period was 5.64 ± 7.2 Tg C y⁻¹, with strong inter and intra-annual variability. The inter-annual variability (2010: -10.13 ± 7.74 Tg C y⁻¹; 2011: 0.35 ± 5.57 Tg C y⁻¹; 2012: 5.86 ± 6.65 Tg C y⁻¹; 2013: 8.90 ± 7.29 Tg C y⁻¹; 2014: 19.27 ± 9.94 Tg C y⁻¹) can largely be explained by the extreme climatic events previously discussed. In early austral summer of 2010, a strong El Niño event started followed by a La Niña in the austral winter [Marengo *et al.*, 2011], along with an anomalous warming of the SST in the northern Atlantic [Espinoza *et al.*, 2011]. All these events combined led to a severe drought in 2010 and the lower river discharge can be clearly observed in hydrology curve (Figure 1b). The Amazon River became disconnected from some streams and floodplains due to the unusually low river discharge, resulting in lower inputs of CO₂ and organic matter. The CO₂ produced in the plume is mostly from the decomposition of river dissolved organic matter by bacteria in the river [Ward *et al.*, 2013] or the very early stages of the plume [Medeiros *et al.*, 2015; Seidel *et al.*, 2015]. Thus the low outgassing flux during 2010 in the ARP is a consequence of the low discharge of the river to the ocean. Additionally, the reduced discharge likely resulted in a reduction of turbidity (i.e. lower suspended sediments concentrations), allowing more light penetration that enhances the primary production and precedes an increase of CO₂ uptake. Smith and Demaster [1996] showed that phytoplankton photosynthesis in waters influenced by the Amazon River is limited by low levels of available irradiance, particularly in the reaches of the plume closest to the river influence [Medeiros *et al.*, 2015].

In contrast, the years of 2012-2014 was marked by an unprecedented flood that started in 2012 associated with La Niña event and continued due to SST anomalies in the western tropical Pacific and in the subtropical South Atlantic [Satyamurty *et al.*, 2013; Espinoza *et al.*, 2014; Marengo and Espinoza, 2016]. During the rising water period of 2014, the rainfall in the southwestern Amazon was 80-100% above normal [Espinoza *et al.*, 2014] and the increase in rainfall throughout the Amazon basin flushed the forest and floodplains and increased the input of organic matter and CO₂ from streams and floodplains into the mainstem. For example, Neu *et al.* [2016] showed that dissolved organic and inorganic carbon fluxes from above ground flow paths (e.g. rainfall, throughfall, stemflow, and overland flow) and stream flow were greater in the Amazon forest during the first large rainfall event after a long dry period. Likewise, Ward *et al.* [2012] observed a similar phenomenon in the temperate Northwest Pacific with dissolved organic carbon (DOC) and vascular plant biomarker (i.e. lignin phenols) concentrations increasing linearly with river discharge during rain events following long dry periods. The increased rainfall that started in 2012 caused a record discharge of the Amazon River to the ocean with highly turbid waters, as observed in the discharge curve (Figure 1b).

Medeiros *et al.* [2015] and Seidel *et al.* [2015] assessed the fate of organic matter along the Amazon River continuum and elucidated the processes and their spatial variability in the ARP. Very close to the mouth, or where the water is more brackish with less light penetration, the predominant process was bacterial remineralization that releases CO₂ to the water. During 2012-2014 the annual flux of CO₂ was positive, suggesting that the greater load of turbid riverine water transported by the ARP interfered with the growth of phytoplankton, reducing the primary production and therefore reducing the oceanic uptake of CO₂. Very brackish water is a better

environment for bacterial respiration, that produces CO₂ and during high levels of river discharge the region of the plume that supports net heterotrophy versus net autotrophy is extended outward from the river mouth.

The annual CO₂ flux from the ARP calculated here differs from *Ibáñez et al.* (2016) (-7.85 ± 1.02 Tg C y⁻¹), and this could be explained by two facts: 1) climatic events that intensified the rainfall at the basin during our study period, leading to a higher discharge water at the ocean and; 2) our work has more sampling points comprising the entire plume, particularly in regions of the plume closer to the Amazon River mouth. *Ibáñez et al.* (2016) collected in situ samples to generate the model to estimate pCO₂ in higher latitudes (14°N 5°N 52°W 41°W) (*Ibáñez et al.*, 2015) where the riverine water was more diluted by marine waters and supports phytoplankton blooms that leads to enhanced CO₂ sinking. During the five-year period, the average minimum carbon flux was -19.24 Tg C y⁻¹, which is close to estimations by *Subramaniam et al.* (2008) of a net Carbon sink of -27 Tg C y⁻¹. The inter-annual variability was marked by a large carbon sink during the high water season of 2010 and high carbon emissions during the rising and high water seasons of 2014 (Table 7).

Table 7. Statistics for the CO₂ flux (Tg C y⁻¹) for the Amazon River Plume.

| Year | Seasonal Discharge | Min | Max | Mean |
|------|--------------------|--------|-------|--------------------|
| 2010 | High | -73.24 | -1.92 | -15.00 ± 11.52 |
| | Falling | -49.00 | -0.65 | -10.95 ± 8.84 |
| | Low | -32.22 | -1.42 | -4.45 ± 2.86 |
| 2011 | Rising | -0.61 | 25.17 | 12.99 ± 5.02 |
| | High | -18.78 | 18.96 | 1.05 ± 5.84 |
| | Falling | -39.18 | 11.12 | -9.62 ± 5.84 |
| | Low | -15.90 | 3.07 | -3.02 ± 1.81 |
| 2012 | Rising | 2.54 | 43.92 | 17.34 ± 6.13 |
| | High | -24.99 | 50.19 | 16.63 ± 13.86 |
| | Falling | -18.51 | 21.09 | -6.33 ± 5.19 |
| | Low | -8.31 | 2.57 | -4.21 ± 1.40 |
| 2013 | Rising | 7.02 | 30.55 | 18.25 ± 4.46 |
| | High | -24.39 | 66.81 | 25.65 ± 17.86 |
| | Falling | -26.82 | 12.53 | -7.98 ± 4.18 |
| | Low | -11.64 | 6.04 | -0.33 ± 2.65 |
| 2014 | Rising | 7.3 | 66.22 | 35.61 ± 9.43 |
| | High | -8.74 | 85.41 | 47.16 ± 20.83 |
| | Falling | -23.2 | 24.68 | -4.70 ± 6.69 |
| | Low | -6.97 | 10.23 | -0.98 ± 2.80 |

4 Conclusions

Based on an empirical relationship between in situ $p\text{CO}_2$ and SMOS-derived SSS and SST was possible to estimate the $p\text{CO}_2$ for the WTNA by remote sensing. Considering the wide range of the driver variable, especially the SSS, our algorithm also faced a weak relationship between the range of ~ 500 – $750 \mu\text{atm}$ and we suggest for future works, especially in the region very close to the shore under more influence of freshwater, to use a different approach, more flexible, e.g., non-linear regression methods (Rödenbeck *et al.*, 2015).

The algorithm that we present here used a microwave sensor that has the advantage of weather independence, essentially, the presence of clouds. Although it has a poor spatial resolution (0.5°) compared to visible sensors ($< 4 \text{ km}$), the $p\text{CO}_2$ average showed a low coefficient of variation within each pixel. However, one drawback is that SMOS products don't go closer to the shoreline due to adjacency effects of land contamination while this coastal region is crucial for understanding the turning point of the CO_2 flux along the Amazon Continuum. For example, as our study pointed out, the mean annual fluxes from the ARP may be also a major net source to the atmosphere if the coastal regions are fully considered. For this, we are attentive for the continue of this study, and willing to consider the use of a visible sensor (e.g. Medium Resolution Imaging Spectrometer - MERIS, Moderate Resolution Imaging Spectroradiometer - MODIS, Visible Infrared Imaging Radiometer Suite - VIIRS, Ocean and Land Colour Instrument - OLCI), not only to approach the coastal region, but also to go upstream into the river. Furthermore, the utilization of visible sensors allows the combination of a diversity of ocean-color products to estimate the $p\text{CO}_2$ such as CDOM and chlorophyll.

SSS was the most important proxy for $p\text{CO}_2$ in the ARP and although visible sensors don't have a salinity product, it is possible to derive a synthetic salinity by the strong negative linear relationship between the absorption coefficients of colored dissolved organic matter and salinity in river plume dominated coastal oceans (Moller *et al.*, 2010). However, to use optical data in the study area would require a very accurate atmospheric correction of satellite images, as well as an effective cloud masking due to high turbidity normally observed in the region. High concentrations of suspended sediments have a high signal response which could be erroneously taken as a cloud. Additionally, this is a significantly cloudy region that would limit the quality and/or quantity of imagery availability.

A limitation faced in our work is the poor performance of SMOS to retrieve low values of salinity. As we advance into the river mouth the error of SSS increased (this was propagated in our calculations). Further, various in situ salinity samples had to be discarded after an outlier analysis with the SMOS products. For the Amazon River, a good agreement was observed between river discharge data and $p\text{CO}_2$ and this relationship was applied to the years of 2010–2014. For all seasons, the studied region presented higher values of $p\text{CO}_2$, and the year of 2010 presented exceptionally low values due to the extreme drought that happened in this year.

It was possible to observe the variability of the CO_2 fluxes during the discharge seasons for the Amazon continuum. The intra-variability of the $F_{\text{CO}_2}^{\text{river}}$ was a consequence of the rainfall season, and therefore the discharge of the river. The $F_{\text{CO}_2}^{\text{sea}}$ responded to both river discharge and plume pathways, which are tied to NBC, NECC and trade winds. During the high water season when

the river is emitting and exporting more CO₂, the plume also sinks less or even emits and exports CO₂. During the falling water season, the river exported less CO₂ compared to the high water season along with less organic matter export. Moreover, the plume is deflected eastward by the NECC and as the extent of the plume gets bigger, the resultant retroflexion drives riverine nutrient export that enhances biological uptake. Thus, the falling water season was ubiquitously a net sink of carbon.

In general, both river and ARP acted as a source of CO₂. Actually, our study period was marked by climatic events and the ARP acted as a sink during the falling and low water period but the total of sinked CO₂ was less when compared to the total of CO₂ emitted during the rising and high water season. The five-year period focused on here were very contrasting, with the drought of 2010 and the flood of 2012-2014, and this was reflected in the behavior of both the river and the plume. The Amazon River emitted less CO₂ during 2010 and more during 2014 and the ARP absorbed more CO₂ during 2010 and took up less during 2014. Results from this study provide enhanced spatial coverage of CO₂ fluxes in the Amazon River, particularly in regions closer to the river, revealing that the ARP is less of a carbon sink than originally thought, and for our study period, acted as a source of CO₂. Perhaps the ARP could be an even major source if the entire coastal extent of the plume is considered in future studies.

Further, we highlight the importance of large-scale climate patterns on carbon cycling across the river to ocean continuum in the world's largest river system.

Conflicts of Interest

The authors declare that the research was conducted in the absence of any commercial or financial relationships that could be construed as a potential conflict of interest.

Funding

This work was supported by the Gordon and Betty Moore Foundation Marine Microbial Initiative River-Ocean Continuum of the Amazon project (GBMF#2293 and GBMF#2928), FAPESP Grant #08/58089-9, NSF DEB Grant #1256724, CNPQ # 303715/2015-4 and CAPES PhD fellowship of AV (#33010013005P0).

Acknowledgments

We thank Diani Fernanda da Silva, Joel Estevão, Vania Neu, William Gagne-Maynard, Daimio Brito, and Rodrigo da Silva for continued participation in the lower Amazon River sampling. We appreciate the exchange of ideas with João Felipe dos Santos and Marcelo Gomes from the National Institute for Space Research during the development of the manuscript. We would also like to thank the captains, crew, and science team of the R/V Knorr, R/V Melville, and R/V Atlantis for their support to the scientific goals of the ANACONDAS (Amazon Influences on the Atlantic: Carbon Export from Nitrogen Fixation by Diatom Symbioses) and ROCAS (River Ocean Continuum of the Amazon) project. We would also like to thank the Ocean Salinity Expertise Center (CECOS) of the CNES-IFREMER Centre Aval de Traitement des Données SMOS (CATDS), at IFREMER (Plouzane, France) for the daily composite, half degree

resolution SMOS SSS and the CarbonTracker from NOAA ESRL, USA, for the Barbados Ragged Point atmosphere pCO₂ time-series data.

References

- Abril, G. et al. (2014), Amazon River carbon dioxide outgassing fuelled by wetlands., *Nature*, 505(7483), 395–8, doi:10.1038/nature12797.
- Alin, S. R., M. D. F. F. L. Rasera, C. I. Salimon, J. E. Richey, G. W. Holtgrieve, A. V. Krusche, and A. Snidvongs (2011), Physical controls on carbon dioxide transfer velocity and flux in low-gradient river systems and implications for regional carbon budgets, *J. Geophys. Res. Biogeosciences*, 116(1), doi:10.1029/2010JG001398.
- Bai, Y., W.-J. Cai, X. He, W. Zhai, D. Pan, M. Dai, and P. Yu (2015), A mechanistic semi-analytical method for remotely sensing sea surface pCO₂ in river-dominated coastal oceans: A case study from the East China Sea, *J. Geophys. Res. Ocean.*, 120, 1–19, doi:10.1002/2014JC010632.Received.
- Borges, A. V., B. Delille, L.-S. Schiettecatte, F. Gazeau, G. Abril, and M. Frankignoulle (2004), Gas transfer velocities of CO₂ in three European estuaries (Randers Fjord, Scheldt, and Thames), *Limnol. Oceanogr.*, 49(5), 1630–1641, doi:10.4319/lo.2004.49.5.1630.
- Brito, D. C. (2013), Balanço de carbono e modelagem de fluxos biogeoquímicos no continuum do estuário amazônico, Universidade Federal do Amapá (UNIFAP).
- Cole, J. J. et al. (2007), Plumbing the global carbon cycle: Integrating inland waters into the terrestrial carbon budget, *Ecosystems*, 10(1), 171–184, doi:10.1007/s10021-006-9013-8.
- Coles, V. J., M. T. Brooks, J. Hopkins, M. R. Stukel, P. L. Yager, and R. R. Hood (2013), The pathways and properties of the Amazon river plume in the tropical North Atlantic Ocean, *J. Geophys. Res. Ocean.*, 118(12), 6894–6913, doi:10.1002/2013JC008981.
- Cooley, S. R., V. J. Coles, A. Subramaniam, and P. L. Yager (2007), Seasonal variations in the Amazon plume-related atmospheric carbon sink, *Global Biogeochem. Cycles*, 21(3), 1–15, doi:10.1029/2006GB002831.
- Dagg, M., R. Benner, S. Lohrenz, and D. Lawrence (2004), Transformation of dissolved and particulate materials on continental shelves influenced by large rivers: plume processes, *Cont. Shelf Res.*, 24(7–8), 833–858, doi:10.1016/j.csr.2004.02.003.
- Espinoza, J. C., J. Ronchail, J. L. Guyot, C. Junquas, P. Vauchel, W. Lavado, G. Drapeau, and R. Pombosa (2011), Climate variability and extreme drought in the upper Solimões River (western Amazon Basin): Understanding the exceptional 2010 drought, *Geophys. Res. Lett.*, 38(13), 1–6, doi:10.1029/2011GL047862.
- Espinoza, J. C., J. A. Marengo, J. Ronchail, J. M. Carpio, L. N. Flores, and J. L. Guyot (2014), The extreme 2014 flood in south-western Amazon basin: the role of tropical-subtropical South Atlantic SST gradient, *Environ. Res. Lett.*, 9(12), 124007, doi:10.1088/1748-9326/9/12/124007.

- Frankignoulle, M., A. Borges, and R. Biondo (2001), A new design of equilibrator to monitor carbon dioxide in highly dynamic and turbid environments, *Water Res.*, *35*(5), 1344–1347, doi:10.1016/S0043-1354(00)00369-9.
- Goes, J. I. et al. (2014), Influence of the Amazon River discharge on the biogeography of phytoplankton communities in the western tropical north Atlantic, *Prog. Oceanogr.*, *120*, 29–40, doi:10.1016/j.pocean.2013.07.010.
- Grodsky, S. a., G. Reverdin, J. a. Carton, and V. J. Coles (2014), Year-to-year salinity changes in the Amazon plume: Contrasting 2011 and 2012 Aquarius/SACD and SMOS satellite data, *Remote Sens. Environ.*, *140*, 14–22, doi:10.1016/j.rse.2013.08.033.
- Hales, B., P. G. Strutton, M. Saraceno, R. Letelier, T. Takahashi, R. Feely, C. Sabine, and F. Chavez (2012), Satellite-based prediction of pCO₂ in coastal waters of the eastern North Pacific, *Prog. Oceanogr.*, *103*, 1–15, doi:10.1016/j.pocean.2012.03.001.
- Hedges, J. I., R. G. Keil, and P. Aransas (1997), What happens to terrestrial organic matter in the ocean?, *Org. Geochem.*, *27*(5), 195–212, doi:10.1016/0146-6380(97)00036-9.
- Ibáñez, J. S. P., D. Diverrès, M. Araujo, and N. Lefèvre (2015), Seasonal and interannual variability of sea-air CO₂ fluxes in the tropical Atlantic affected by the Amazon River plume, *Global Biogeochem. Cycles*, *28*(9), 1–16, doi:10.1002/2015GB005110.
- Ibáñez, J. S. P., M. Araujo, and N. Lefèvre (2016), The overlooked tropical oceanic CO₂ sink, *Geophys. Res. Lett.*, *43*(8), 3804–3812, doi:10.1002/2016GL068020.
- Landschützer, P., N. Gruber, D. C. E. Bakker, and U. Schuster (2014), Recent variability of the global ocean carbon sink, *Glob. Planet. Change*, 927–949, doi:10.1002/2014GB004853.Received.
- Lauerwald, R., G. Laruelle, J. Hartmann, P. Ciais, and P. A. G. Regnier (2015), Spatial patterns in CO₂ evasion from the global river network, *Global Biogeochem. Cycles*, *29*, 1–21, doi:10.1002/2014GB004941.
- Lefèvre, N., D. Diverrès, and F. Gallois (2010), Origin of CO₂ undersaturation in the western tropical Atlantic, *Tellus, Ser. B Chem. Phys. Meteorol.*, *62*(5), 595–607, doi:10.1111/j.1600-0889.2010.00475.x.
- Lentz, S. J., and R. Limeburner (1995), The Amazon River Plume during AMASSEDs: Subtidal current variability and the importance of wind forcing, *J. Geophys. Res.*, *100*(C2), 2355–2375, doi:10.1029/94JC01411.
- Lohrenz, S. E., and W.-J. Cai (2006), Satellite ocean color assessment of air-sea fluxes of CO₂ in a river-dominated coastal margin, *Geophys. Res. Lett.*, *33*(1), L01601, doi:10.1029/2005GL023942.
- Marengo, J. A., and J. C. Espinoza (2016), Extreme seasonal droughts and floods in Amazonia: Causes, trends and impacts, *Int. J. Climatol.*, *36*(3), 1033–1050, doi:10.1002/joc.4420.
- Marengo, J. A., J. Tomasella, L. M. Alves, W. R. Soares, and D. A. Rodriguez (2011), The

- drought of 2010 in the context of historical droughts in the Amazon region, *Geophys. Res. Lett.*, 38(12), 1–5, doi:10.1029/2011GL047436.
- Mecklenburg, S. et al. (2012), ESA's soil moisture and ocean salinity mission: Mission performance and operations, *IEEE Trans. Geosci. Remote Sens.*, 50(5 PART 1), 1354–1366, doi:10.1109/TGRS.2012.2187666.
- Medeiros, P. M., M. Seidel, N. D. Ward, E. J. Carpenter, H. R. Gomes, J. Niggemann, A. V. Krusche, J. E. Richey, P. L. Yager, and T. Dittmar (2015), Fate of the Amazon River dissolved organic matter in the tropical Atlantic Ocean, *Global Biogeochem. Cycles*, 29, 1–14, doi:10.1002/2015GB005115.
- Moller, G. S. F., E. M. L. d. M. Novo, and M. Kampel (2010), Space-time variability of the Amazon River plume based on satellite ocean color, *Cont. Shelf Res.*, 30(3–4), 342–352, doi:10.1016/j.csr.2009.11.015.
- Neu, V., N.D. Ward, A.V. Krusche and C. Neill (2016) Dissolved organic and inorganic carbon flow paths in an Amazonian transitional forest, *Frontiers in Marine Science*. 3 (114). doi: 10.3389/fmars.2016.00114.
- Nohara, D., A. Kitoh, M. Hosaka and T. Oki (2006). Impact of climate change on river discharge projected by multimodel ensemble. *J. Hydrometeor.* 7, 1076–1089.
- Rasera, M. de F. F. L., A. V. Krusche, J. E. Richey, M. V. R. Ballester, and R. L. Victória (2013), Spatial and temporal variability of pCO₂ and CO₂ efflux in seven Amazonian Rivers, *Biogeochemistry*, 116(1–3), 241–259, doi:10.1007/s10533-013-9854-0.
- Raymond, P. A. et al. (2013), Global carbon dioxide emissions from inland waters, *Nature*, 503(7476), 355–359, doi:10.1038/nature12760.
- Reul, N., J. Tenerelli, J. Boutin, B. Chapron, F. Paul, E. Brion, F. Gaillard, and O. Archer (2012), Overview of the first SMOS sea surface salinity products. Part I: Quality assessment for the second half of 2010, *IEEE Trans. Geosci. Remote Sens.*, 50(5 PART 1), 1636–1647, doi:10.1109/TGRS.2012.2188408.
- Richey, J. E., J. I. Hedges, A. H. Devol, P. D. Quay, R. Victoria, L. Martinelli, and B. R. Forsberg (1990), Biogeochemistry of carbon in the Amazon River, *Limnol. Oceanogr.*, 35(2), 352–371.
- Richey, J. E., J. M. Melack, A. K. Aufdenkampe, V. M. Ballester, and L. L. Hess (2002), Outgassing from Amazonian rivers and wetlands as a large tropical source of atmospheric CO₂, *Nature*, 416(1991), 617–620, doi:10.1038/416617a.
- Rödenbeck, C. et al. (2015), Data-based estimates of the ocean carbon sink variability - First results of the Surface Ocean pCO₂ Mapping intercomparison (SOCOM), *Biogeosciences*, 12(23), 7251–7278, doi:10.5194/bg-12-7251-2015.
- Satyamurty, P., C. P. W. Da Costa, A. O. Manzi, and L. A. Candido (2013), A quick look at the 2012 record flood in the Amazon Basin, *Geophys. Res. Lett.*, 40(7), 1396–1401, doi:10.1002/grl.50245.

- Smith, W. O., and D. J. Demaster (1996), Phytoplankton biomass and productivity in the Amazon River plume: correlation with seasonal river discharge, *Cont. Shelf Res.*, 16(3), 291–319, doi:10.1016/0278-4343(95)00007-N.
- Sawakuchi, H.O., V. Neu, N.D. Ward, M.L.C. Barros, A.M. Valerio, W. Gagne- Maynard, A. C. Cunha, D.F.S. Less, J.E.M. Diniz, D.C. Brito, A.V. Krusche, and J.E. Richey, Carbon dioxide emissions along the lower Amazon River. *Frontiers Marine Science* (in review).
- Seidel, M., P.L. Yager, N.D. Ward, E.J. Carpenter, H.R. Gomes, A.V. Krusche, J.E. Richey, T. Dittmar, and P.M. Medeiros (2015), Molecular-level changes of dissolved organic matter along the Amazon River-to-Ocean continuum of the Amazon. *Marine Chemistry*. 177(2), 218-231.
- Subramaniam, A., P.L. Yager, E.J. Carpenter, C. Mahaffey, K. Björkman, S. Cooley, A.B. Kustka, J.P. Montoya, S.A. Sañudo-Wilhelmy, R. Shipe, and D.G. Capone (2008), Amazon River enhances diazotrophy and carbon sequestration in the tropical North Atlantic Ocean., *Proc. Natl. Acad. Sci. U. S. A.*, 105(30), 10460–5, doi:10.1073/pnas.0710279105.
- Talone, M., A. Camps, B. Mourre, R. Sabia, M. Vall-llossera, J. Gourrion, C. Gabarró, and J. Font (2009), Simulated SMOS Level 2 and 3 products: The effect of introducing argo data in the processing chain and its impact on the error induced by the vicinity of the coast. *IEEE Trans. Geosci. Remote Sens.* 47, 3041-3050.050.
- Ternon, J. F., C. Oudot, A. Dessier, and D. Diverrés (2000), A seasonal tropical sink for atmospheric CO₂ in the Atlantic ocean : the role of the Amazon River discharge, *Mar. Chem.*, 68, 183–201.
- Tranvik, L. J., J. A. Downing, J. B. Cotner, S. A. Loiselle, R. G. Striegl, T. J. Ballatore, P. Dillon, K. Finlay, K. Fortino, and L. B. Knoll (2009), Lakes and reservoirs as regulators of carbon cycling and climate, *Limnol. Oceanogr.*, 54(6, part 2), 2298–2314, doi:10.4319/lo.2009.54.6_part_2.2298.
- Wanninkhof, R. (1992), Relationship Between Wind Speed and Gas Exchange, *J. Geophys. Res.*, 97(92), 7373–7382, doi:10.1029/92JC00188.
- Wanninkhof, R. (2014), Relationship between wind speed and gas exchange over the ocean revisited, *Limnol. Oceanogr. Methods*, 12, 351–362, doi:10.1029/92JC00188.
- Ward, N.D., J.E. Richey, R.G. Keil (2012), Temporal variation in river nutrient and dissolved lignin phenol concentrations and the impact of storm events on nutrient loading to Hood Canal, Washington, USA. *Biogeochemistry*. 111(1-3), 629-645.
- Ward, N. D., Keil, R. G., Medeiros, P. M., Brito, D. C., Cunha, A. C., Dittmar, T., *et al.* (2013). Degradation of terrestrially derived macromolecules in the Amazon River. *Nature Geoscience*. 6(7), 530-533.
- Ward, N. D., A. V. Krusche, H. O. Sawakuchi, D. C. Brito, A. C. Cunha, J. M. S. Moura, R. da Silva, P. L. Yager, R. G. Keil, and J. E. Richey (2015), The compositional evolution of

dissolved and particulate organic matter along the lower Amazon River-Óbidos to the ocean, *Mar. Chem.*, 177, 244–256, doi:10.1016/j.marchem.2015.06.013.

Ward, N.D., Bianchi, T.S., Sawakuchi, H.O., Gagne-Maynard, W., Cunha, A.C., Brito, D.C., *et al.* (2016). The reactivity of plant-derived organic matter and the potential importance of priming effects in the lower Amazon River. *Journal of Geophysical Research: Biogeosciences*. 121, 1522-1539.

Weiss, R. F. (1974), Carbon dioxide in water and seawater: the solubility of a non-ideal gas, *Mar. Chem.*, 2, 203–215.

Yeung, L. Y. et al. (2012), Impact of diatom-diazotroph associations on carbon export in the Amazon River plume, *Geophys. Res. Lett.*, 39(18), L18609, doi:10.1029/2012GL053356.

Zhu, Y., S. Shang, W. Zhai, and M. Dai (2009), Satellite-derived surface water pCO₂ and air-sea CO₂ fluxes in the northern South China Sea in summer, *Prog. Nat. Sci.*, 19(6), 775–779, doi:10.1016/j.pnsc.2008.09.004.